The Astrophysical Journal, 578:64–73, 2002 October 10

FAR-ULTRAVIOLET SPECTROSCOPIC EXPLORER OBSERVATIONS OF THE NARROW-LINE SEYFERT 1 GALAXY ARAKELIAN 564[1]

P. Romano,[2] S. Mathur,[2] R. W. Pogge,[2] B. M. Peterson,[2] and J. Kuraszkiewicz[3]

Received 2002 April 8; accepted 2002 June 18

ABSTRACT

We present a 63 ks *FUSE* observation of the narrow-line Seyfert 1 galaxy Arakelian 564. The spectrum is dominated by the strong emission in the O VI $\lambda\lambda1032$, 1038 resonance doublet. Strong, heavily saturated absorption troughs due to Lyman series of hydrogen, O VI, and C III $\lambda977$ at velocities near the systemic redshift of Ark 564 are also observed. We used the column densities of O VI and C III, in conjunction with the published column densities of species observed in the UV and X-ray bands, to derive constraints on the physical parameters of the absorber through photoionization modeling. The available data suggest that the UV and X-ray absorbers in Ark 564 are physically related and possibly identical. The combination of constraints indicates that the absorber is characterized by a narrow range in total column density $N_{\rm H}$ and U, centered at $\log N_{\rm H} \approx 21$ and $\log U \approx -1.5$, and may be spatially extended along the line of sight.

Subject headings: galaxies: active — galaxies: individual (Arakelian 564) — galaxies: nuclei — galaxies: Seyfert — ultraviolet: galaxies

On-line material: color figures

1. INTRODUCTION

More than half of the Seyfert 1 population show optical/UV intrinsic absorption associated with their active nuclei (Crenshaw et al. 1999 and references therein). The strong UV absorption lines, Lyα, C IV, and N V (and less frequently Si IV and Mg II), are found to be blueshifted, or at rest, with respect to the narrow emission lines, providing an important indication of the presence of a net radial outflow of the absorbing gas. A similar percentage also show an associated ionized ("warm") X-ray absorber (George et al. 1998; Reynolds 1997) that is characterized by high ionization, $U = 0.1$–10 ($U = Q/4\pi r^2 n_{\rm H} c$, where Q is the number of ionizing photons), and high total hydrogen column density, $N_{\rm H} = 10^{21}$–10^{23} cm^{-2}, which signature is typically the presence of O VII and O VIII edges. During the last decade evidence has been accumulated indicating that the same gas is responsible for the absorption in the UV and X-ray spectra of Seyfert 1 galaxies (Mathur 1994; Mathur et al. 1994; Mathur, Elvis, & Wilkes 1995; Crenshaw et al. 1999; Kriss et al. 2000; Monier et al. 2001; Brotherton et al. 2002). Although it is not always possible to model the X-ray and UV absorbers as a single zone (especially when the complex UV absorption is resolved in multiple velocity components that are characterized by a large range of column densities and ionization), common characteristics of these absorbers have emerged, i.e., they are composed of high-ionization, low-density, high column density gas that is outflowing and is located in or outside the broad emission line region (BELR). It is therefore worthwhile to investigate the nature of this nuclear component in active galactic nuclei (AGNs), which represents an outflow (or wind) that can carry away a significant amount of kinetic energy at a mass-loss rate comparable to the accretion rate required to fuel the AGN (Mathur et al. 1995).

Arakelian 564 (IRAS 22403+2927, MCG +05-53-012) is a bright, nearby, narrow-line Seyfert 1 (NLS1) galaxy, with $z = 0.02467$, $V = 14.6$ mag (de Vaucouleurs et al. 1991), and $L_{2-10\ {\rm keV}} = 2.4 \times 10^{43}$ ergs s^{-1} (Turner et al. 2001, hereafter Paper I). It was the object of an intense multiwavelength monitoring campaign that included simultaneous observations from *ASCA* (2000 June 1 to July 6; Paper I; Pounds et al. 2001; Edelson et al. 2002), *Hubble Space Telescope* (*HST*; 2000 May 9 to July 8; Collier et al. 2001, hereafter Paper II; Crenshaw et al. 2002, hereafter Paper IV), and many ground-based observatories, as part of an AGN Watch[4] project (1998 November to 2001 January; Shemmer et al. 2001, hereafter Paper III). Ark 564 has shown a strong associated UV absorber (Crenshaw et al. 1999; Paper II; Paper IV). There are indications that it also possesses a warm X-ray absorber, as seen by the absorption lines of O VII and O VIII detected in a *Chandra* spectrum (Matsumoto, Leighly, & Marshall 2001).[5]

In this paper, we present the results from a 63 ks *Far-Ultraviolet Spectroscopic Explorer* (*FUSE*) observation of Ark 564 obtained on 2001 June 29–30 UT, focusing in particular on the O VI intrinsic absorption; we investigate the physical properties of the UV and X-ray absorbing gas, using the constraints on column densities obtained during the multiwavelength observations of this AGN. In § 2 we present the data. In § 3 we describe our analysis methods. In § 4 we test the hypothesis that the warm UV and X-ray absorbers are one and the same through photoionization calculations. In § 5 we discuss some implications of our investigation. Our results are summarized in § 6. In a forthcoming paper (P. Romano et al. 2002, in preparation), we

[1] Based on observations made with the NASA-CNES-CSA *Far-Ultraviolet Spectroscopic Explorer*. *FUSE* is operated for NASA by Johns Hopkins University under NASA contract NAS5-32985.

[2] Department of Astronomy, Ohio State University, 140 West 18th Avenue, Columbus, OH 43210-1173; promano@astronomy.ohio-state.edu, mathur@astronomy.ohio-state.edu, pogge@astronomy.ohio-state.edu, peterson@astronomy.ohio-state.edu.

[3] Harvard-Smithsonian Center for Astrophysics, 60 Garden Street, MS 83, Cambridge, MA 02138; jkuraszkiewicz@cfa.harvard.edu.

[4] All publicly available data and complete references to published AGN Watch papers can be found at http://www.astronomy.ohio-state.edu/~agnwatch.

[5] See http://www.pha.jhu.edu/groups/astro/workshop2001/papers.

will analyze the intrinsic spectral energy distribution (SED) of Ark 564 and the properties of the gas responsible for the broad emission lines.

2. OBSERVATIONS AND DATA REDUCTION

We observed Ark 564 with *FUSE* (Moos et al. 2000; Sahnow et al. 2000) for 63 ks, starting on 2001 June 29 07:37:42 UT. The observations, consisting of 24 separate exposures, were performed in photon address (time-tag) mode through the $30'' \times 30''$ low-resolution (LWRS) aperture. During our observation, a high-voltage anomaly occurred, and detector 1 did not collect useful data during the first eight exposures. To best model the background for this observation, we first used the task TTAG_COMBINE, provided with the *FUSE* calibration pipeline CALFUSE (version 2.0.5),[6] to combine the last 16 exposures for detector 1 (total exposure of 42 ks) and all 24 exposures for detector 2. We then processed the combined exposures with the standard pipeline and extracted spectra from both detectors. The flux scale for the final spectra is accurate to $\pm 10\%$, while the wavelength scale is accurate to ± 15 km s^{-1}. As a result of the high-voltage anomaly and data screening, the effective on-source times were 41 ks in detector 1A, 39 ks in detector 1B, 58 ks in detector 2A, and 62 ks in detector 2B. Consequently, the SiC1A and SiC1B spectra were discarded from further analysis, the final signal-to-noise ratio (S/N) being $\lesssim 1.5$, even at 0.6 Å (100 pixels) resolution. We also discarded the LiF1B spectrum, since it showed wavelength-dependent differences in flux of up to 30%–50% compared to the LiF1A spectrum, probably due to the "worm," which cannot be corrected for by the pipeline (Oegerle, Murphy, & Kriss 2000, p. 42).

The full *FUSE* spectrum was obtained by combining the spectra extracted from the SiC2A, LiF2B, LiF1A, SiC2B, and LiF2A segments, yielding a wavelength coverage of 916–1175 Å. We then rebinned the full spectrum in a linear wavelength scale using 0.07 Å bins (10 pixels, here on our high-resolution spectrum, with an effective resolution of 20 km s^{-1}), 0.2 Å bins (30 pixels, medium-resolution spectrum), and 0.6 Å bins (100 pixels, low-resolution spectrum).

Figure 1 shows the low-resolution spectrum after we cosmetically removed the strong airglow lines (mainly H I Lyman series, O I λ989, O I λ1027, and He I λ584, seen in second order at 1167 Å) and C III λ977, which is scattered solar light in the SiC detector. The main spectral features are identified, the most prominent being the emission lines of the O VI $\lambda\lambda$1032, 1038 resonance doublet. Strong absorption features due to Lyβ and O VI $\lambda\lambda$1032, 1038 at velocities near the redshift of Ark 564 are also observed. We detect absorption from Galactic interstellar medium (ISM) molecular hydrogen, mainly H_2 Lyman series absorption (see Shull et al. 2000, Sembach et al. 2000, and Savage et al. 2000), and atomic Galactic ISM lines, including O VI $\lambda\lambda$1032, 1038 (S. Mathur et al. 2002, in preparation). No intrinsic Lyman edge is detected.

3. DATA ANALYSIS

Our goal was to determine the column densities of the ionic species we observed in our spectrum, combine this

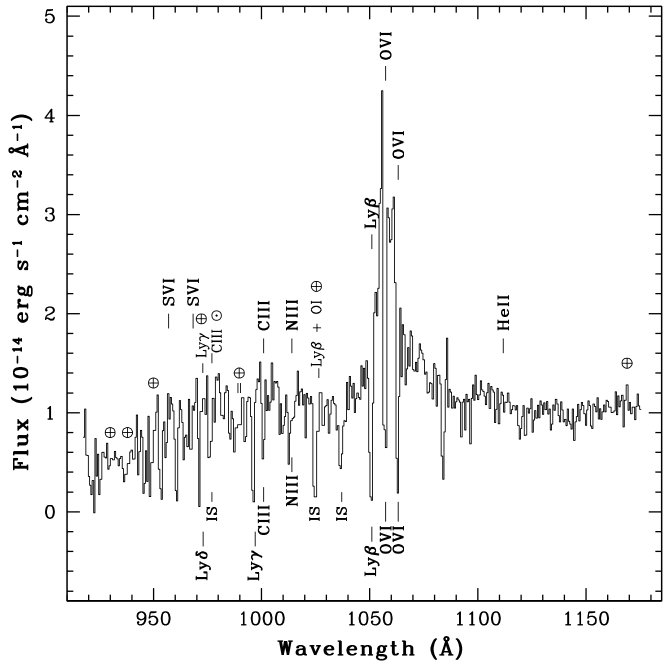

FIG. 1.—*FUSE* spectrum of Ark 564, binned to a resolution of 0.6 Å (100 pixels). In addition to the prominent emission lines from the O VI $\lambda\lambda$1032, 1038 resonance doublet, we suggest identifications for the main emission and absorption features. The strong airglow lines (H I Lyman series, O I λ989, O I λ1027, and He I λ584, seen in second order at 1167 Å) and the C III λ977 line (which is scattered solar light in the SiC detector) have been removed. All other absorption features are due to Galactic or intergalactic absorption (indicated with "IS"). The absorption feature at $\sim$1080 Å is partially due to a gap between detectors.

information with the column densities available in the literature for Ark 564, and derive constraints on the physical parameters of the absorber (total density and ionization) through photoionization modeling. *HST* Faint Object Spectrograph spectra of Ark 564 (Crenshaw et al. 1999) show the presence of strong intrinsic absorption lines of Lyα, N V $\lambda\lambda$1238.8, 1242.8, Si IV $\lambda\lambda$1393.8, 1402.8, and C IV $\lambda\lambda$1548.2, 1550.8. Of these lines, which are resolved in Space Telescope Imaging Spectrograph (STIS) spectra into multiple components (Paper II; Paper IV), Lyα, N V, and C IV are completely saturated. Figure 2 shows the *FUSE* high-resolution (0.07 Å, 10 pixels) spectrum of Ark 564, in the Lyβ/O VI wavelength region. Close examination of the O VI troughs shows that the lines are heavily saturated and that their shape is mainly determined by partial covering effects (see § 3.2 and Fig. 3 below). Therefore, the absorption lines are not resolved into components at different velocities with respect to the systemic velocity, we must treat each of the absorption troughs as a single absorption component, and we can only determine the velocity-averaged column densities of the observed species. We note, however, that O VI λ1032 is not completely black. Indeed, analysis of the spectra obtained with different pulse height restrictions and from night-only data (we did not use the latter for this work, since the lower S/N did not allow a proper subtraction of Galactic molecular hydrogen) shows that scattered light is marginal in this observation and that there is no filling in of the absorption troughs. It is also clear that the uncertainty in the measurement of O VI absorption-line parameters, and hence O VI column density, is dominated by the uncertainty in the underlying emission-line profile. In addition, there is

[6] See http://fuse.pha.jhu.edu/analysis/calfuse.html.

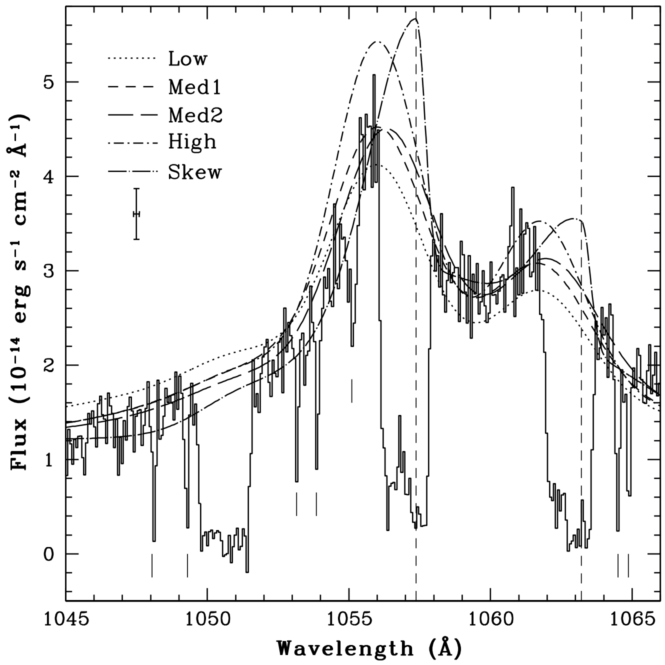

FIG. 2.—High-resolution (0.07 Å, ∼10 pixels) spectrum of Ark 564 in the Lyβ/O VI wavelength region. The dashed vertical lines mark the rest-frame wavelengths of the O VI lines, and the short vertical lines mark Galactic absorption lines. Overlaid are our five adopted models for the combined continuum and emission lines: low-lying (Low), medium (Med1 and Med2), high-lying (High, which best follows the O VI λ1038 peak), and a model with skewed Gaussian emission lines (Skew). All absorption lines are saturated, but while Lyβ and O VI λ1038 are black, O VI λ1032 is not. The mean 1 σ error bar on the spectrum is also shown for reference. [*See the electronic edition of the Journal for a color version of this figure.*]

contamination from absorption lines of Galactic molecular hydrogen, with a column density log $N(H_2) \gtrsim 16$ (K. R. Sembach 2002, private communication); this is not surprising, given the substantial amount of neutral atomic hydrogen ($N_H = 6.4 \times 10^{20}$ cm^{-2}; Dickey & Lockman 1990) along the line of sight toward Ark 564. Given these limitations, we proceeded as follows: we determined a power-law continuum underlying the Lyβ/O VI wavelength region using the low-resolution spectrum (S/N $\lesssim$ 15 in the continuum); we then modeled the Lyβ and O VI emission lines from the high- and medium-resolution spectra (S/N $\lesssim$ 10 in the emission lines for high resolution) and used H_2 templates to estimate the H_2 contribution to the O VI absorption troughs. This part of the analysis was done using the IRAF[7] task SPECFIT (Kriss 1994) in the STSDAS package. Finally, we measured the absorption-line parameters of the normalized line profiles, using the high-resolution spectrum, and determined the column densities with the apparent optical depth method, which we briefly describe below (§ 3.2).

3.1. *Intrinsic* O VI *Emission Models*

In addition to the power-law continuum (which we kept fixed relative to the fit of the low-resolution spectrum), our models for the adopted "continuum" under the absorption troughs included a pair of broad O VI emission lines (FWHM = 4000–5000 km s^{-1}), a pair of narrow O VI emission lines (FWHM = 1000–1100 km s^{-1}), and a broad and a narrow Lyβ emission line. All lines are taken to have Gaussian profiles. The intensity of the O VI doublet lines was fixed to the optically thin value 2 : 1 for both broad and narrow lines, while their wavelengths were linked to the ratio of their laboratory values; the FWHM and wavelength of the broad Lyβ line were linked to those of the O VI lines, although a small shift in wavelength was permitted, consistent with increasing blueshift with respect to the systemic velocity as the ionization increases.

To assess the possible range of absorption-line parameters, we considered five different models for the emission lines, shown in Figure 2. In the first four models, low-lying (Low), medium (Med1 and Med2), and high-lying (High, which best follows the O VI λ1038 peak, although it clearly overpredicts the O VI λ1032 peak), the Gaussian profiles for the emission lines were symmetrical. As observed in many AGNs (see, e.g., Marziani et al. 1996), the emission lines in all our models are blueshifted with respect to the systemic redshift, $z_e = 0.02467$, as derived from H I measurements (de Vaucouleurs et al. 1991), by 390–1240 km s^{-1}. Finally, we considered a model in which the broad lines have the least blueshift (100 km s^{-1}) with respect to the systemic redshift and the narrow lines are at the systemic redshift; in this case, in order to model the profile, the narrow emission lines must be highly asymmetrical (Skew model; skewness = 0.2). The motivation for considering the last model is the increasing evidence that the high-ionization emission lines in NLS1's are broader and present an excess of flux in the blue with respect to the low-ionization lines (Laor et al. 1997b; Peterson et al. 2000; Mathur 2000; Leighly 2001 and references therein). With our choice of Low, Med1, Med2, and High emission-line profiles, the absorption is redshifted with respect to the emission lines. This is highly unusual, although not unprecedented (Mathur, Elvis, & Wilkes 1999; Goodrich 2000). When the emission is modeled with the Skew profile, the absorption is in part blueshifted and in part redshifted with respect to the emission lines. Table 1 lists the O VI model emission-line parameters. Since no inflection points are clearly seen in the observed emission-line profiles, our models may not have a direct physical interpretation. Also, while we believe the true shape of the emission-line profile may be most realistically represented by the Med1 and Med2 profiles, we consider the most extreme profiles (Low, High, and Skew) to bracket the constraints on the values of column density.

Our spectrum also shows narrow H_2 and H I absorption lines from the ISM in the Lyβ/O VI wavelength region; in particular, the top panel of Figure 3 shows six such absorption lines that lie outside the absorption troughs, which we fitted as Gaussians with SPECFIT (FWHM = 30 km s^{-1}). We then used H_2 and H I absorption-line templates (S. McCandliss 2001, private communication; K. R. Sembach 2002, private communication) to predict the position of the lines in the absorption troughs and derive their intensity by scaling them to the two lines at ∼1065 Å. Incidentally, we note a 0.115 Å shift between the predicted and observed wavelengths of H_2 absorption lines. The amount of this shift is constant along our spectrum; hence, we interpreted it as a residual zero-point offset in the wavelength calibration of our spectrum; as reported in many

[7] IRAF is distributed by the National Optical Astronomy Observatory, which is operated by the Association of Universities for Research in Astronomy, Inc., under cooperative agreement with the National Science Foundation.

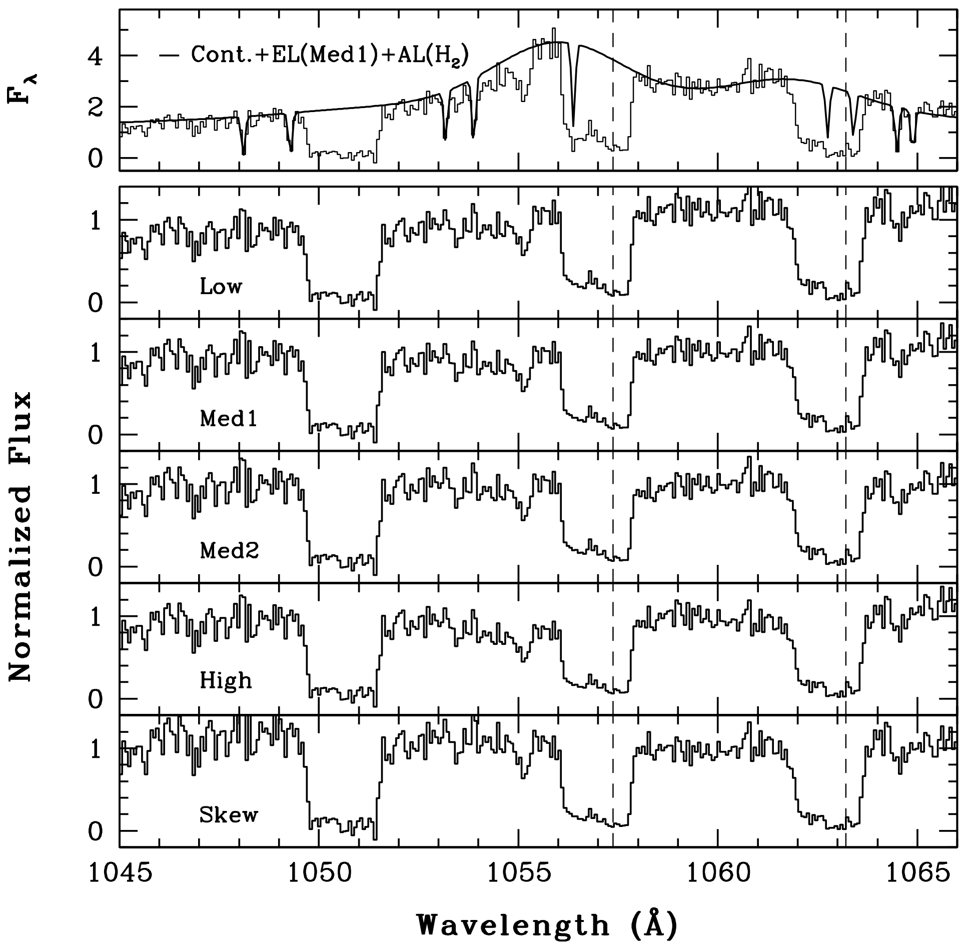

FIG. 3.—*Top*: High-resolution spectrum of Ark 564 in the Lyβ/O VI wavelength region, with a model for the continuum, the emission lines (Med1), and molecular hydrogen absorption lines overlaid as a thick solid curve [log $N(H_2) \sim 10^{16}$]. The other panels show the normalized line profiles of the absorption system at $z_a \approx z_e$. The dashed vertical lines mark the rest-frame wavelengths of the O VI lines. [*See the electronic edition of the Journal for a color version of this figure.*]

observations,[8] these offsets can be as high as 0.25 Å in the LWRS aperture. We matched templates and spectra accordingly. Figure 3 shows the line profiles normalized with respect to the combined continuum, emission-line, and H_2 profiles for the five different O VI emission-line models.

3.2. *Intrinsic* O VI *Absorption Measurements*

As mentioned above, the O VI lines are so heavily saturated that we must treat each of the absorption troughs as a single absorption component (as opposed to the many components observed in Si IV and Si III λ1206.5; Paper IV). This assumption is only strictly valid if the physical conditions are approximately constant along the line profile, i.e., as a function of radial velocity. We considered the possibility of partial covering of the lines and used the apparent optical depth method to determine the column densities. Following Hamann et al. (1997), we calculated the lower limit to the line-of-sight covering factor C_f from the residual intensities I_r in the troughs as a function of radial velocity and the corresponding apparent optical depth τ,

$$C_f \geq 1 - \frac{I_r}{I_0} \tag{1}$$

and

$$\tau \geq \ln\left(\frac{I_0}{I_r}\right) , \tag{2}$$

where I_0 is the assumed continuum intensity across the absorption line (in the case of O VI, I_0 is our combined power-law continuum and emission-line models corrected for the Galactic hydrogen absorption, as described in § 3.1). Column densities are then obtained by integrating the apparent optical depth across the line profile with

$$N_{\rm ion} \geq \frac{m_e c}{\pi e^2 f \lambda} \int \tau(v)\ dv \tag{3}$$

(see, e.g., Savage & Sembach 1991), where λ and f are the laboratory wavelength and oscillator strength of the transition, respectively.

Figure 4 shows the normalized line profiles, the covering factor, and the optical depth as a function of radial velocity relative to the systemic redshift, $z_e = 0.02467$, for the Med1 emission-line profile. Predictably, $C_f \approx 1$ for most of the

[8] See http://fuse.pha.jhu.edu/analysis/calfuse_wp1.html.

TABLE 1
O VI MODEL EMISSION-LINE PARAMETERS

Model (1)	Line (2)	λ[a] (Å) (3)	Flux[a] (10^{-13} ergs s^{-1} cm^{-2}) (4)	FWHM (km s^{-1}) (5)	ΔV[b] (km s^{-1}) (6)
Low	BEL O VI λ1032	1053	1.00	5000	−1240
	BEL O VI λ1038	1058.82	0.50	5000	−1240
	NEL O VI λ1032	1056	0.90	1100	−390
	NEL O VI λ1038	1061.83	0.45	1100	−390
Med1	BEL O VI λ1032	1055	1.00	4000	−670
	BEL O VI λ1038	1060.83	0.50	4000	−670
	NEL O VI λ1032	1056	1.00	1100	−390
	NEL O VI λ1038	1061.83	0.50	1100	−390
Med2	BEL O VI λ1032	1056	1.00	4000	−390
	BEL O VI λ1038	1061.83	0.50	4000	−390
	NEL O VI λ1032	1056.3	1.00	1100	−300
	NEL O VI λ1038	1062.13	0.50	1100	−300
High.........	BEL O VI λ1032	1055	1.00	4000	−670
	BEL O VI λ1038	1060.83	0.50	4000	−670
	NEL O VI λ1032	1056	1.25	1000	−390
	NEL O VI λ1038	1061.83	0.63	1000	−390
Skew	BEL O VI λ1032	1057	1.25	2000	−100
	BEL O VI λ1038	1062.84	0.63	2000	−100
	NEL O VI λ1032	1057.37	0.60	1000	0
	NEL O VI λ1038	1063.21	0.30	1000	0

[a] Observed values.
[b] Velocities are relative to the systemic redshift $z_e = 0.02467$ (H I measurements; de Vaucouleurs et al. 1991). The shift toward longer wavelengths of 0.115 Å to match the Galactic molecular hydrogen templates is not included.

O VI λ1038 profile and is consistent with unity for O VI λ1032. The arrows show the position of the zero velocity with respect to the BELs and NELs. As noted in § 3.1, while most of the absorption is blueshifted with respect to the systemic redshift, the absorption troughs are completely, or at least partially (Skew model), redshifted with respect to the BELs and NELs. The absorption troughs also show the presence of gas that is redshifted with respect to the systemic velocity. This may indicate that the absorbing gas is undergoing net radial infall, as is the case for NGC 5548 (Mathur et al. 1999) and RX J0134−42 (Goodrich 2000).

We used $\log f\lambda = 2.137$ for O VI λ1032 and $\log f\lambda = 1.836$ for O VI λ1038 (Morton 1991). Table 2 reports the values of O VI column densities for our five assumed emission-line models; $N_{\rm O\,VI} = [2.31, 2.65] \times 10^{15}$ cm^{-2} and $[5.28, 5.96] \times 10^{15}$ cm^{-2} when measured from O VI λ1032 and O VI λ1038, respectively. The errors quoted in Table 2 are relative to the measurement of the integral of τ in velocity space only. We estimate that molecular hydrogen lines contribute ∼10% to the flux in the absorption troughs. We adopt $(5.7 \pm 0.07) \times 10^{15}$ cm^{-2}, obtained by averaging the values from Med1 and Med2 emission-line models for the O VI λ1038 line, as a conservative lower limit on the O VI column density.

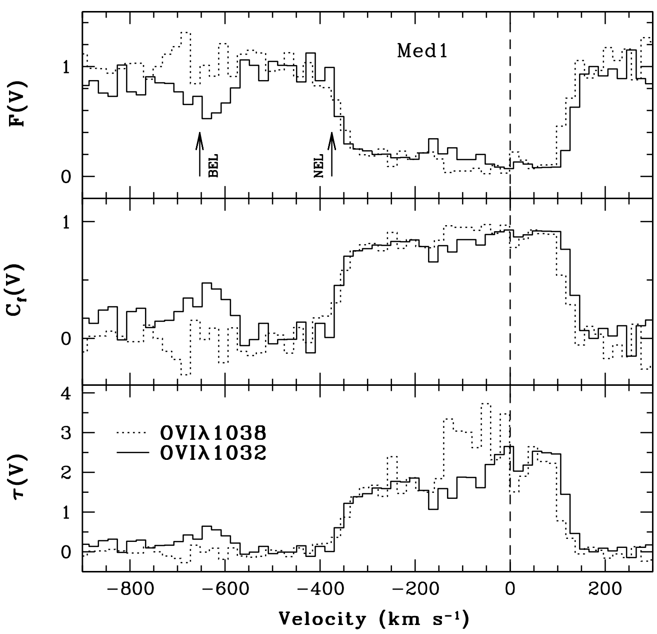

FIG. 4.—*Top*: Normalized line profiles (Med1 model) of the absorption system as a function of radial velocity, relative to a systemic redshift $z_e = 0.02467$ (H I). Arrows show the position of the zero velocity with respect to the broad emission lines (BELs) and narrow emission lines (NELs). *Middle*: Covering factor as a function of radial velocity. *Bottom*: Optical depth as a function of radial velocity. Solid lines refer to the O VI λ1032 profile and dotted lines to the O VI λ1038 profile.

3.3. C III *Column Density*

We also determined the column density of C III from the C III λ977 absorption trough with the apparent optical depth method described in § 3.2 ($\log f\lambda = 2.872$; Morton 1991). The Lyγ/C III wavelength region does not necessarily require the same degree of complication in the emission-line profile as the Lyβ/O VI wavelength region; however, although we performed fits and measurements separate from the Lyβ/O VI ones, for consistency we adopted the same emission model as Med2, albeit with different flux normalization: one broad (FWHM = 4000 km s^{-1}) and one narrow (FWHM = 1100 km s^{-1}) Gaussian emission line for

TABLE 2

O VI COLUMN DENSITIES FROM INTRINSIC ABSORPTION

Line (1)	Low Model (10^{15} cm^{-2}) (2)	Med1 Model (10^{15} cm^{-2}) (3)	Med2 Model (10^{15} cm^{-2}) (4)	High Mode (10^{15} cm^{-2}) (5)	Skew Model (10^{15} cm^{-2}) (6)
O VI λ1032.......	2.31 ± 0.03	2.47 ± 0.05	2.54 ± 0.03	2.65 ± 0.03	2.80 ± 0.03
O VI λ1038.......	5.28 ± 0.05	5.60 ± 0.05	5.77 ± 0.05	5.96 ± 0.05	5.64 ± 0.05

NOTE.—The errors quoted are relative to the measurement of the integral of τ in velocity space only. We estimate that molecular hydrogen lines contribute ~10% to the flux in the absorption troughs.

C III and one broad Lyγ Gaussian emission line; the FWHM and wavelength of the broad Lyγ line were linked to those of the broad C III line. We obtained a C III column density of $(3.19 \pm 0.05) \times 10^{14}$ cm^{-2} (errors are relative to the measurement of the integral of τ in velocity space only, while a 10% contribution is due to molecular hydrogen absorption lines).

3.4. *Velocity Centroids*

Table 3 reports the values of the radial velocity centroids relative to the systemic redshift of the O VI, C III, Lyβ, and Lyγ absorption lines, along with the measured column densities. We also show the results of Paper IV, to emphasize the good agreement between the centroid velocity shifts (relative to systemic redshift) obtained for the H I Lyman series in the *FUSE* and in the *HST* spectra. In Paper IV, it is also noted that while saturation is probably responsible for the discrepancy in the values of the centroids in the different ions, the most saturated lines, i.e., the H I Lyman series, give us an estimate of the total coverage of the absorber. Paper IV reports a range [−420, +180] km s^{-1} for Lyα, and we obtain [−431, +174] km s^{-1} for Lyβ, [−412, +147] km s^{-1} for Lyγ, [−395, +177] km s^{-1} for C III, and [−412, +130] km s^{-1} for O VI λ1038. The less saturated O VI λ1032 yields [−374, +142] km s^{-1}. Our *FUSE* spectrum was obtained a year after the last of the *HST*/STIS spectra were taken, and we confirm the finding of Paper IV that there are no changes in radial velocity coverage of the absorber.

4. PHOTOIONIZATION MODELING

It is common practice to use photoionization codes to predict the fractional abundance of an element in a given ionization state, $f_{\rm ion}$, given an input continuum, density n, total column density $N_{\rm H}$, and ionization parameter U of the gas. The fractional abundance of an ion of an element X is related to its column density $N_{\rm ion}$ and the abundance of its element $N_{\rm X}$ by $N_{\rm ion} = N_{\rm H} N_{\rm X} f_{\rm ion}$, which provides a prediction of $N_{\rm ion}$ that can be tested against observations. We used CLOUDY (version 94.00; Ferland 1996)[9] to calculate $f_{\rm ion}$ for the ionic species for which we measured column densities from the *FUSE* spectrum and for the species with published column densities, which are reported for easy reference in Table 3. We considered a range of values of $N_{\rm H}$ for a range of input continua (described in detail in § 4.1) and a total

[9] See http://www.pa.uky.edu/~gary/cloudy.

TABLE 3

COLUMN DENSITIES FROM INTRINSIC ABSORPTION IN ARK 564

Ion (1)	Wavelength/Energy (2)	Lower Limit (cm^{-2}) (3)	Detection (cm^{-2}) (4)	Upper Limit (cm^{-2}) (5)	Velocity (km s^{-1}) (6)	References (7)
H I............	973 Å	...	...	...	−108	1
C III	977.0 Å	3.2×10^{14}	...	...	−153	1
H I............	1025 Å	...	...	...	−111	1
O VI..........	1031.9, 1037.6 Å	5.7×10^{15}[a]	...	...	−79/−116	1
Si III..........	1206.5 Å	...	2.6×10^{13}	...	−190	2
H I............	1216 Å	1.4×10^{15}	...	...	−106	2
N V...........	1238.8, 1242.8 Å	3.1×10^{15}	...	...	−152	2
Si II...........	1260.4 Å	...	...	7.4×10^{13}	...	2
C II	1334.5 Å	...	...	5.4×10^{13}	...	2
Si IV..........	1393.8, 1402.8 Å	...	1.6×10^{14}	...	−197	2
C IV	1548.2, 1550.8 Å	2.5×10^{15}	...	...	−130	2
O VII[b]	0.74 keV	...	...	2.2×10^{17}	...	2
O VIII[b]	0.87 keV	...	...	1.1×10^{16}	...	2

NOTE.—Col. (1): Ion. Col. (2): Wavelength of absorption lines or energy of absorption edges. Col. (3): Lower limit on column densities, as derived from line-fitting/apparent optical depth methods. Col. (4): Column density values derived using the multiplet method of Hamann et al. 1997. Col. (5): Upper limit on column densities, as derived from nondetection of the line. Col. (6): Velocity centroids relative to the systemic redshift $z_e = 0.02467$. Col. (7): References for column densities and velocity centroids.

[a] Average of values obtained from Med1 and Med2 emission-line models.

[b] Absorption edge.

REFERENCES.—(1) This work. (2) Paper IV.

hydrogen density of 10^5 cm^{-3}, and we assumed solar abundances relative to hydrogen. In the case of "table AGN," we specified a grid of N_H- and U-values. For all other models, we normalized the SEDs with respect to the measured X-ray luminosity in the absorption-corrected rest-frame 2–10 keV energy range ($L_{2-10\ \mathrm{keV}} = 2.4 \times 10^{43}$ ergs s^{-1}; Paper I) and specified the radius of the cloud, thus obtaining U. We note that the use of the observed SEDs assumes that the absorbing gas sees the same ionizing continuum as the observer does.

4.1. *Input Continua*

Figure 5 illustrates our choices of input continua for CLOUDY:

1. The CLOUDY "table AGN" continuum, which is the Mathews & Ferland (1987) continuum modified with a submillimeter break at 10 μm, so that the spectral index is changed from -1 to $-5/2$ (specific flux $F_\nu \propto \nu^{-\alpha}$) for frequencies below the millimeter break. While "table AGN" is unlikely to be a representative SED for Seyfert galaxies, we use this continuum for comparison with the literature.

2. A combination of the SED described in Laor et al. (1997a) and Zheng et al. (1997) for radio-quiet objects (LZ in Fig. 5). We have extended the original SED in Laor et al. (1997a) to cover the whole 10^{-5} to 7.354×10^6 ryd energy range, as required by CLOUDY. We defined a submillimeter break at the low energies and a break at 100 keV (with a spectral index of $-5/3$) at the high energies, analogous to the ones in "table AGN." This "composite" continuum might be a typical AGN continuum.

3. Observed SEDs. We used data obtained during the multiwavelength monitoring campaign performed in 2000, which included simultaneous observations of Ark 564 from *ASCA* (Paper I), *HST* (Paper II), and many ground-based observatories (Paper III). In addition, *IRAS* measurements (Moshir et al. 1990) and our *FUSE* observations have been used. While the full extent of the data is used to create a quasi-simultaneous SED (P. Romano et al. 2002, in preparation), our adopted continuum for CLOUDY only consists of selected points (also shown in Fig. 5). All data have been corrected for redshift. Special care has been paid in correcting the data for reddening, given the indications (Paper IV) that strong, intrinsic, neutral absorption is present in Ark 564 in excess of the Galactic absorption. Therefore, we corrected the spectra for reddening in two different ways:

a) using a standard Galactic extinction curve with $E(B-V) = 0.06$ mag (Schlegel, Finkbeiner, & Davis 1998) (SED1 in Fig. 5); and

b) using a standard Galactic extinction curve with $E(B-V) = 0.03$ mag, plus the intrinsic extinction curve that Crenshaw et al. (Paper IV) derive for Ark 564 with $E(B-V) = 0.14$ mag (SED2 in Fig. 5). In the *FUSE* band we extrapolated the extinction correction linearly from the one relative to the *HST* band. We also note that to match our *FUSE* spectrum and *HST* spectrum in the overlapping region, we had to scale the *FUSE* fluxes by 0.75. This is not inconsistent with a combination of effects, such as flux intercalibration uncertainties and, most importantly, source flux variability.

In the X-ray, we used continuum points from the power-law fit (photon index $\Gamma = \alpha + 1 = 2.538$) and added a blackbody component of temperature $T = 1.8 \times 10^6$ K and luminosity $L_{bb} = 2.48 \times 10^{38}$ ergs s^{-1}, as derived from fits to the mean *ASCA* spectrum. The squares in Figure 5 denote the adopted points for SED1 and the circles those for SED2, while the horizontal lines show the full ranges where data were available. The full details of the observed SED, as well as the analysis of the properties of the BELR gas, will be presented in P. Romano et al. (2002, in preparation).

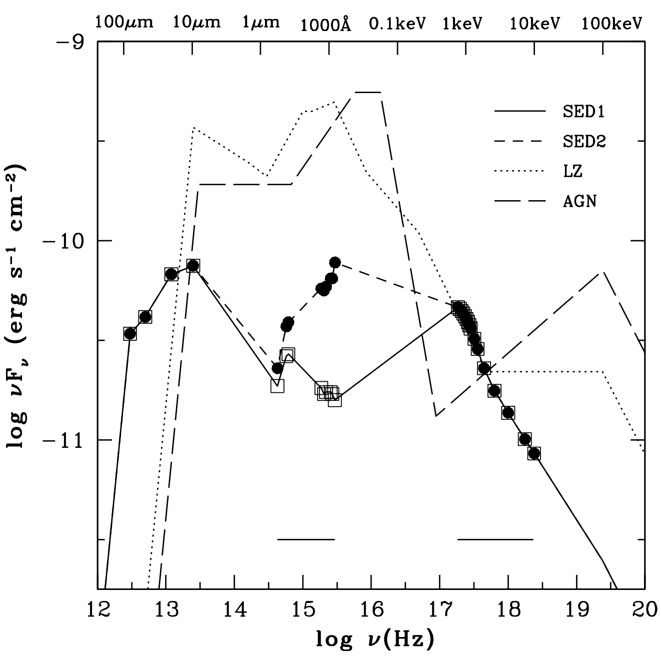

FIG. 5.—Comparison of the adopted SEDs for Ark 564, normalized to the absorption-corrected rest-frame flux at 2 keV. The long-dashed line shows the "table AGN" model in CLOUDY; the dotted line shows the ionizing continuum described in Laor et al. (1997a) and Zheng et al. (1997); the solid line shows the Ark 564 SED described in P. Romano et al. (2002, in preparation), which is based on data corrected for reddening with a standard Galactic extinction curve and $E(B-V) = 0.06$; the short-dashed line shows the Ark 564 ionizing continuum based on data corrected for reddening with both a standard Galactic extinction curve and $E(B-V) = 0.03$ and the intrinsic extinction curve derived for Ark 564 in Paper IV and $E(B-V) = 0.14$. Squares denote adopted points for SED1 and circles those for SED2, while the horizontal lines show the full ranges where data were available. [*See the electronic edition of the Journal for a color version of this figure.*]

4.2. *Physical Conditions of the UV/X-Ray Absorber*

Following Arav et al. (2001), we constrain the characteristics of the absorber by plotting curves of constant N_{ion} on the log U–log N_H plane. In this plane, for each constant N_{ion} curve, lower limits on the column densities, derived from apparent optical depth line-fitting methods, exclude the area below it, while upper limits, derived from nondetections, exclude the area above it. Figure 6 shows the N_{ion} constraints (see Table 3) for the "table AGN" input continuum and solar abundances. Lower limits are shown as solid lines, upper limits as dashed lines, and detections as dotted lines. The combination of constraints given by the column densities suggests that the absorber in Ark 564 is characterized by a narrow range in N_{ion} and U, i.e., $\log U = [-1.74, -0.74]$ and $\log N_H = [19.90, 21.89]$. We note the consistency of all constraints without departure from solar abundances. Analogously, Figure 7 shows the N_{ion} constraints for our SED1 input continuum and indicates

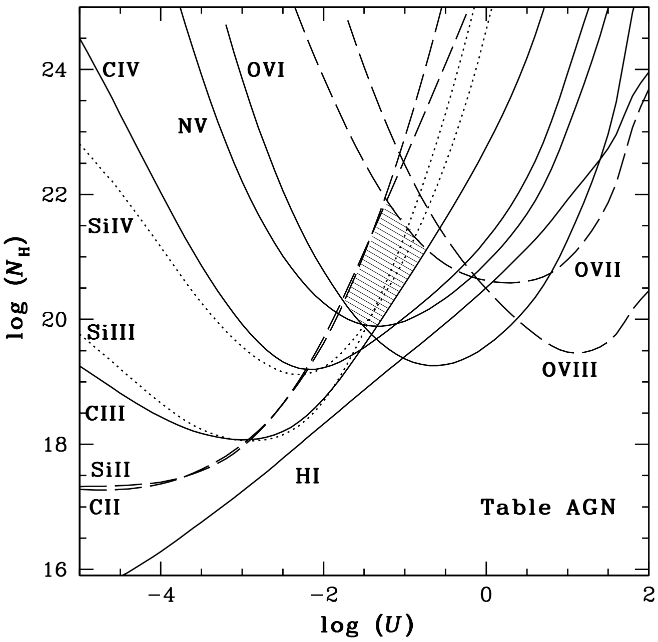

FIG. 6.—Photoionization curves at constant ionic column density on the plane of total hydrogen column density $N_{\rm H}$ vs. ionization parameter U. The shape of the ionizing radiation is defined by the "table AGN" model in CLOUDY, and the abundances are solar. Lower limits are shown as solid lines, upper limits as dashed lines, and detections as dotted lines. For clarity, curves relative to ions of the same element have been drawn in the same color: C in red, O in light blue, and Si in dark blue. The shaded region corresponds to the locus on the log U–log $N_{\rm H}$ space where all conditions are met (see § 4.2), i.e., where $\log U = [-1.74, -0.74]$ and $\log N_{\rm H} = [19.90, 21.89]$. [*See the electronic edition of the Journal for a color version of this figure.*]

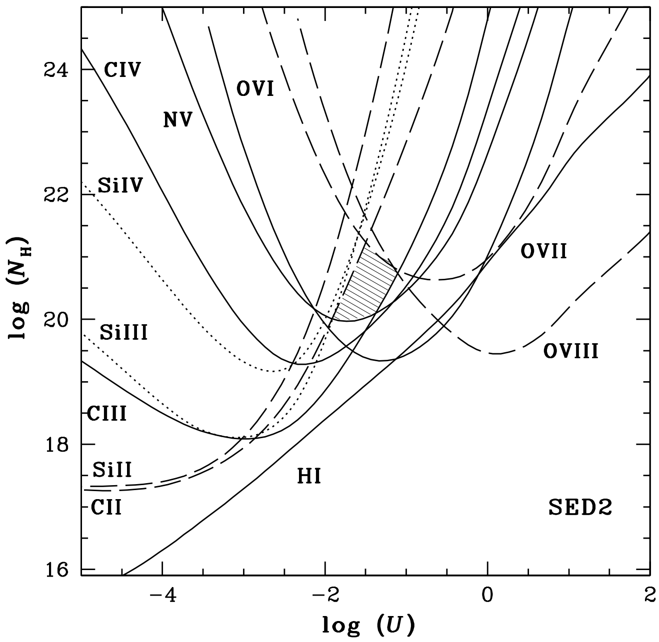

FIG. 8.—Same as Fig. 6, but with an ionizing continuum with Galactic and intrinsic reddening (SED2 in Fig. 5). Most constraints are met in $\log U = [-1.86, -1.02]$ and $\log N_{\rm H} = [19.95, 21.27]$ (see § 4.2). [*See the electronic edition of the Journal for a color version of this figure.*]

$\log U = [-1.99, -1.31]$ and $\log N_{\rm H} = [19.99, 21.09]$, and Figure 8 (SED2 continuum) indicates $\log U = [-1.86, -1.02]$ and $\log N_{\rm H} = [19.95, 21.27]$, while Figure 9 (LZ continuum) indicates $\log U = [-1.97, -1.54]$ and $\log N_{\rm H} = [20.00, 20.79]$. Thus, depending on the input continuum, there are small but significant differences in the derived properties of the absorber.

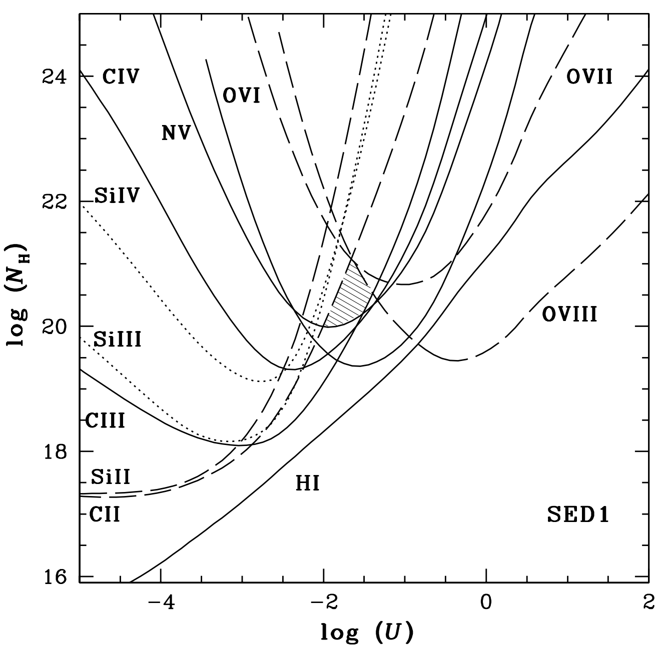

FIG. 7.—Same as Fig. 6, but with an ionizing continuum with no reddening intrinsic to Ark 564 (SED1 in Fig. 5). Most constraints are met in $\log U = [-1.99, -1.31]$ and $\log N_{\rm H} = [19.99, 21.09]$ (see § 4.2). [*See the electronic edition of the Journal for a color version of this figure.*]

5. DISCUSSION

The UV absorber in Ark 564 is in a general state of outflow with respect to the systemic redshift (see Table 3). A very good agreement is found between the values of the velocity centroids we derive for the species observed in the *FUSE* spectrum and those derived for the *HST*/STIS spectrum (Paper IV); therefore, we adopt as the best estimate of the net radial velocity of the UV absorber the value obtained in Paper IV for Si III and Si IV, the least saturated lines: $V_{\rm out} = -194 \pm 5$ km s^{-1}. The absorption troughs also show the presence of gas that is redshifted with respect to the systemic velocity. This can be explained in part as a saturation effect, as is shown in Figure 3 of Paper IV. Alternatively, a model with more than one kinematic component is required to explain the observed absorption troughs (e.g., Elvis 2000); in this scenario, in addition to the blueshifted absorption from an outflowing wind, we would be observing redshifted absorption from infalling material, such as an accretion flow. In addition to the continuum source, the absorbing gas must cover a substantial portion of the BELR, since the absorption troughs are much deeper than the continuum level. Assuming the identity of the UV and X-ray–absorbing gas, we have used the column densities of the observed species to constrain the physical conditions of the absorber. For the most realistic SED (SED2), we obtained $\log N_{\rm H} = [19.95, 21.27]$ and $\log U = [-1.86,$

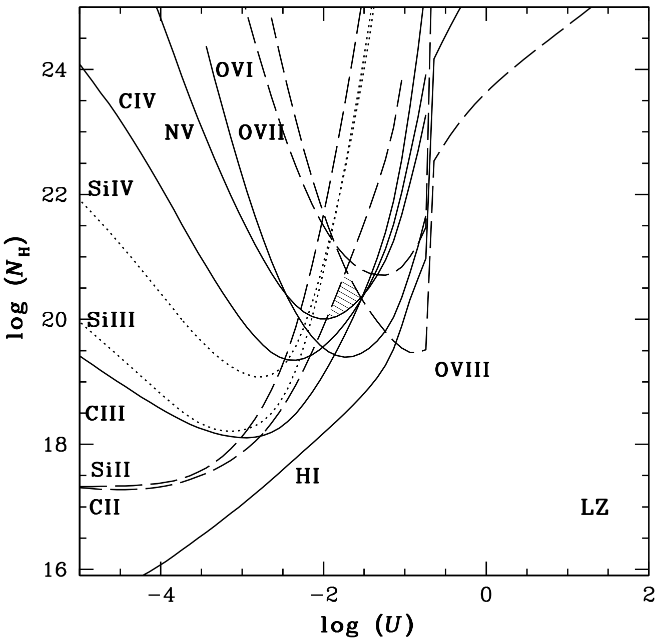

FIG. 9.—Same as Fig. 6, but with an ionizing continuum described in Laor et al. (1997a) and Zheng et al. (1997) (LZ in Fig. 5). Most constraints are met in $\log U = [-1.97, -1.54]$ and $\log N_{\rm H} = [20.00, 20.79]$ (see § 4.2). [*See the electronic edition of the Journal for a color version of this figure.*]

$-1.02]$. These constraints can be used to determine the size of the absorber, its distance from the central continuum source, and the mass outflow rate. For the following order-of-magnitude arguments, we adopt the mean values $U = 0.0363$ and $N_{\rm H} = 4.07 \times 10^{20}$ cm^{-2}. The size of the absorber is derived from the total column density, $r_{\rm abs} = 4.07 \times 10^{20} n_{\rm H}^{-1}$ cm. For SED2 the number of ionizing photons is $Q = 6.68 \times 10^{55}$ s^{-1}, so the distance from the continuum source is $R_{\rm abs} = 7.00 \times 10^{22} n_{\rm H}^{-1/2}$ cm. Using the lower limit on $R_{\rm abs} > 95$ pc found in Paper IV, this would indicate a total density $n_{\rm H} > 5.70 \times 10^4$ cm^{-3}. Assuming uniform density and considering that $r_{\rm abs} \ll R_{\rm abs}$, the mass of the outflowing gas is $M_{\rm abs} = 2.11 \times 10^{10} f n_{\rm H}^{-1}$ $M_\odot$, where f is the covering factor, i.e., the fraction of the sky covered by the absorber as seen at the central source. The mass outflow rate is then $\dot{M}_{\rm abs} = M_{\rm abs} V_{\rm out}/r_{\rm abs} = 3.17 \times 10^4 f$ $M_\odot$ yr^{-1}, and the outflow carries out a rate of kinetic energy $\dot{M}_{\rm abs} V_{\rm out}^2/2 = 3.76 \times 10^{44} f$ ergs s^{-1}. To power Ark 564 at the observed luminosity ($L_{\rm bol} = 10 L_{2\text{–}10\ {\rm keV}} = 2.4 \times 10^{44}$ ergs s^{-1}) at an efficiency $\eta = 0.1$, an accretion rate $\dot{M}_{\rm acc} = 1.8 \times 10^{-3} (L_{44}/\eta) = 4.3 \times 10^{-2}$ $M_\odot$ yr^{-1} is required (L_{44} is the bolometric luminosity in units of 10^{44} ergs s^{-1}).

The outflow carries out a kinetic luminosity about 1 order of magnitude smaller than the observed radiative luminosity of the source. However, the mass outflow rate is uncomfortably large unless the covering factor is very small. If $\dot{M}_{\rm abs} \lesssim \dot{M}_{\rm acc}$, then it implies $f \lesssim 10^{-6}$. Alternatively, our assumption $r_{\rm abs} \ll R_{\rm abs}$ might not be valid. The absorber might be an extended, low-density region. The assumption of a uniform-density gas may not be strictly valid, and the ionization parameter and density that we deduced should only be considered as "average" values. Recent *Chandra* observations have found extended warm gas in some AGNs (Sako et al. 2000) with physical characteristics similar to those of a warm absorber, but seen in emission. So it is quite likely that the warm absorber in Ark 564 is also spatially extended along the line of sight.

In Paper IV, the UV absorber was modeled as a single zone with quasi-solar abundances (carbon depletion being the main departure), and the best-fit values of $\log U = -1.48$ and $\log N_{\rm H} = 21.21$ are consistent with our limits. Paper IV overpredicted carbon and oxygen column densities: $N_{\rm C\ III} = 5.2 \times 10^{15}$ cm^{-2} and $N_{\rm O\ VI} = 2.4 \times 10^{17}$ cm^{-2} (cf. our measurements: $N_{\rm C\ III} = 3.2 \times 10^{14}$ cm^{-2} and $N_{\rm O\ VI} = 5.7 \times 10^{15}$ cm^{-2}). These predictions, however, are consistent with the upper-end values of our range of parameter space. We note that our modeling did not require carbon to be depleted.

Finally, we can compare our solutions of $\log N_{\rm H} = 21$ and $\log U = -1.5$, with the preliminary results of Matsumoto et al. (2001), based on analysis of a 50 ks *Chandra* observation of Ark 564. Their curve-of-growth analysis on the absorption lines indicates that $N_{\rm O\ VII} = 3.2 \times 10^{17}$ cm^{-2}, $N_{\rm O\ VIII} = 1 \times 10^{18}$ cm^{-2}, $N_{\rm Ne\ IX} = 3.2 \times 10^{17}$ cm^{-2}, and $N_{\rm Ne\ X} = 1 \times 10^{17}$ cm^{-2}, suggestive of $\log N_{\rm H} = 21$ and $\log \xi = 1.6$–2. While there is agreement between the values of $\log N_{\rm H}$ and $N_{\rm O\ VII}$, the column densities they measure for O VII do not agree with the ones derived in Paper IV from the upper limits on the bound-free optical depths in the *ASCA* spectrum (Paper I). Given the high $N_{\rm O\ VIII}$, we would expect that an edge would be observable in the *Chandra* spectrum.

6. SUMMARY

We have presented a 63 ks *FUSE* observation of the NLS1 galaxy Ark 564. The observed spectrum is dominated by the O VI $\lambda\lambda$1032, 1038 emission lines. As observed in many AGNs (see, e.g., Marziani et al. 1996), the emission lines in all our models are blueshifted (or at rest, as in the case of our Skew blue asymmetric model) with respect to the systemic redshift by 100–1240 km s^{-1}. Blue asymmetric UV emission-line profiles may be a characteristic of NLS1 galaxies.

We concentrated on the analysis of the strong and heavily saturated absorption troughs due to Lyman series, O VI, and C III λ977, which are observed at velocities near the systemic redshift of Ark 564. In a forthcoming paper (P. Romano et al. 2002, in preparation), we will analyze the intrinsic SED of Ark 564 and the properties of the BELR gas. Using the apparent optical depth method, we have determined that the column density of O VI is a few times 10^{15} cm^{-2} and that $N_{\rm C\ III} = 3.2 \times 10^{14}$ cm^{-2}. We used these values, in conjunction with the published column densities of species observed in the UV and X-ray spectra of this object, to derive constraints on the physical parameters of the UV/X-ray–absorbing gas through photoionization modeling. The combination of constraints, assuming the most realistic SED, indicates that the absorber is characterized by a narrow range of density and ionization parameter, $\log N_{\rm H} = [19.95, 21.27]$ and $\log U = [-1.86, -1.02]$.

There is excellent agreement in the kinematic properties of the UV absorber emerging from the combined analysis of the *FUSE* and *HST*/STIS spectra, i.e., distribution of gas in radial velocity (as derived from the extent of the absorption troughs) and net radial velocity (as derived from the velocity centroids). The UV/X-ray absorber in Ark 564 is in outflow with respect to the systemic redshift, with a radial velocity of a few hundred km s^{-1}, and it is likely spatially extended along the line of sight. The absorption troughs also show the presence of gas that is redshifted with respect to the systemic velocity. This may indicate that a component in the absorbing gas is undergoing net radial infall. This is highly unusual, although not unprecedented (Mathur et al. 1999; Goodrich 2000).

P. R. and S. M. acknowledge support through NASA grant NAG5-10320. We thank the *FUSE* team for the operation of their satellite, and K. R. Sembach and S. McCandliss for sharing their molecular hydrogen absorption templates. We thank S. Vercellone for useful discussions. This research has made use of the NASA/IPAC Extragalactic Database (NED), which is operated by the Jet Propulsion Laboratory, California Institute of Technology, under contract with the National Aeronautics and Space Administration.

REFERENCES

Arav, N., et al. 2001, ApJ, 561, 118
Brotherton, M. S., Green, R. F., Kriss, G. A., Oegerle, W., Kaiser, M. E., Zheng, W., & Hutchings, J. B. 2002, ApJ, 565, 800
Collier, S., et al. 2001, ApJ, 561, 146 (Paper II)
Crenshaw, D. M., Kraemer, S. B., Boggess, A., Maran, S. P., Mushotzky, R. F., & Wu, C.-C. 1999, ApJ, 516, 750
Crenshaw, D. M., et al. 2002, ApJ, 566, 187 (Paper IV)
de Vaucouleurs, G., de Vaucouleurs, A., Corwin, H. G., Jr., Buta, R. J., Paturel, G., & Fouqué, P. 1991, Third Reference Catalogue of Bright Galaxies (New York: Springer)
Dickey, J. M., & Lockman, F. J. 1990, ARA&A, 28, 215
Edelson, R., Turner, T. J., Pounds, K., Vaughan, S., Markowitz, A., Marshall, H., Dobbie, P., & Warwick, R. 2002, ApJ, 568, 610
Elvis, M. 2000, ApJ, 545, 63
Ferland, G. J. 1996, Hazy, a Brief Introduction to CLOUDY 94.00 (Lexington: Univ. Kentucky Dept. Phys. Astron.)
George, I. M., Turner, T. J., Netzer, H., Nandra, K., Mushotzky, R. F., & Yaqoob, T. 1998, ApJS, 114, 73
Goodrich, R. W. 2000, NewA Rev., 44, 519
Hamann, F., Barlow, T. A., Junkkarinen, V., & Burbidge, E. M. 1997, ApJ, 478, 80
Kriss, G. 1994, in ASP Conf. Ser. 61, Astronomical Data Analysis Software and Systems III, ed. D. R. Crabtree, R. J. Hanisch, & J. Barnes (San Francisco: ASP), 437
Kriss, G. A., et al. 2000, ApJ, 538, L17
Laor, A., Fiore, F., Elvis, M., Wilkes, B. J., & McDowell, J. C. 1997a, ApJ, 477, 93
Laor, A., Jannuzi, B. T., Green, R. F., & Boroson, T. A. 1997b, ApJ, 489, 656
Leighly, K. M. 2001, in ASP Conf. Ser. 224, Probing the Physics of Active Galactic Nuclei, ed. B. M. Peterson, R. S. Polidan, & R. W. Pogge (San Francisco: ASP), 293
Marziani, P., Sulentic, J. W., Dultzin-Hacyan, D., Calvani, M., & Moles, M. 1996, ApJS, 104, 37
Mathews, W. G., & Ferland, G. J. 1987, ApJ, 323, 456
Mathur, S. 1994, ApJ, 431, L75
———. 2000, NewA Rev., 44, 469
Mathur, S., Elvis, M., & Wilkes, B. 1995, ApJ, 452, 230
———. 1999, ApJ, 519, 605
Mathur, S., Wilkes, B., Elvis, M., & Fiore, F. 1994, ApJ, 434, 493
Matsumoto, C., Leighly, K. M., & Marshall, H. L. 2001, X-ray Emission from Accretion onto Black Holes, ed. T. Yaqoob & J. H. Krolik (Baltimore: Johns Hopkins Univ.), E46
Monier, E. M., Mathur, S., Wilkes, B., & Elvis, M. 2001, ApJ, 559, 675
Moos, H. W., et al. 2000, ApJ, 538, L1
Morton, D. C. 1991, ApJS, 77, 119
Moshir, M., et al. 1990, *IRAS* Faint Source Catalogue, version 2.0 (Pasadena: IPAC)
Oegerle, W., Murphy, E., & Kriss, G. A. 2000, *FUSE* Data Handbook, version 1.1 (Baltimore: Johns Hopkins Univ.)
Peterson, B. M., et al. 2000, ApJ, 542, 161
Pounds, K., Edelson, R., Markowitz, A., & Vaughan, S. 2001, ApJ, 550, L15
Reynolds, C. S. 1997, MNRAS, 286, 513
Sahnow, D. J., et al. 2000, ApJ, 538, L7
Sako, M., Kahn, S. M., Paerels, F., & Liedahl, D. A. 2000, ApJ, 543, L115
Savage, B. D., & Sembach, K. R. 1991, ApJ, 379, 245
Savage, B. D., et al. 2000, ApJ, 538, L27
Schlegel, D. J., Finkbeiner, D. P., & Davis, M. 1998, ApJ, 500, 525
Sembach, K. R., et al. 2000, ApJ, 538, L31
Shemmer, O., et al. 2001, ApJ, 561, 162 (Paper III)
Shull, J. M., et al. 2000, ApJ, 538, L73
Turner, T. J., Romano, P., George, I. M., Edelson, R., Collier, S. J., Mathur, S., & Peterson, B. M. 2001, ApJ, 561, 131 (Paper I)
Zheng, W., Kriss, G. A., Telfer, R. C., Grimes, J. P., & Davidsen, A. F. 1997, ApJ, 475, 469 (erratum, 492, 855)